Effects of Interface Roughness on Electronic Transport Properties of Nanotube–Molecule–Nanotube Junctions

ARTICLE *in* THE JOURNAL OF PHYSICAL CHEMISTRY C · JUNE 2010

Impact Factor: 4.77 · DOI: 10.1021/jp102945v

4 AUTHORS, INCLUDING:

Xiao-Fei Li
University of Electronic Science and Techn…
53 PUBLICATIONS **417** CITATIONS
SEE PROFILE

Ke-Qiu Chen
Hunan University
158 PUBLICATIONS **2,034** CITATIONS
SEE PROFILE

Yi Luo
KTH Royal Institute of Technology
444 PUBLICATIONS **8,922** CITATIONS
SEE PROFILE

Effects of Interface Roughness on Electronic Transport Properties of Nanotube−Molecule−Nanotube Junctions

Xiao-Fei Li,[†,‡] Ke-Qiu Chen,[†] Lingling Wang,[†] and Yi Luo*[,‡,§]

School of Physics and Microelectronics, Hunan University, Changsha 410082, China, Hefei National Laboratory for Physical Sciences at the Microscale, University of Science and Technology of China, Hefei, Anhui 230026, China, and Department of Theoretical Chemistry, School of Biotechnology, Royal Institute of Technology, S-106 91 Stockholm, Sweden

Received: April 1, 2010; Revised Manuscript Received: April 22, 2010

We investigate electronic transport properties of molecular junctions constructed by a single conjugated molecule attached in the gap of two broken metallic single walled carbon nanotubes (CNTs). With the help of molecular dynamic simulations (MD), we have provided a realistic description for mechanical stretching processes of different carbon nanotubes and contact structures between the broken CNTs and the conjugated molecule in different junctions. Statistical analysis shows that the molecule generally prefers to be titled inside the junctions with polygonal contact, in particular the apex at the broken ends of tubes. Nonequilibrium Green's function (NEGF) calculations reveal that such realistic CNTs-molecular junctions have very different electron transport properties from junctions with ideal SWCNTs as electrodes. The statistically and energetically favorable CNTs-molecular junctions of different chiralities are found to be always metallic, but their absolute conductance is sensitive to the chirality of the tube. It is suggested that with armchair CNTs as electrodes, a better conductivity can be obtained. The calculated current−voltage characteristics of junctions with realistic contact geometries are in good agreement with experiments.

I. Introduction

In the past decade, electron transport properties of metal−molecule junctions have attracted much attention.[1,2] In particular, the carbon nanotubes (CNTs) based metal−CNTs junctions are intensely studied experimentally and theoretically,[3−8] because of their unique one-dimensional geometry, superior mechanical and chemical robustness, and excellent chirality dependent electronic property.[9] Recent theoretical and experimental studies have also explored the use of carbon nanotubes as the tips for atomic force microscopy (AFM)[10,11] and the electrodes for single molecular junctions.[12−16] It is found that the resolution of the AFM image is governed by the geometry details of the apex at the end of the CNT tip,[11] while the electronic transport property of CNTs-molecular junctions is sensitive to the coupling between CNTs and the molecule. In reality, the interface structure is complicated by the fact that the contact areas of CNTs are largely rough as revealed by experimental studies.[17−20] The presence of defects and deformations could greatly complicate the contact details and modify the electronic structure of the molecule, hence change conductance of the system. The ideal CNTs-molecular junctions, in which the CNTs have been cut vertically[5−8,14−16,21] or along a certain inclined plane,[22] have been widely studied. These studies have provided much insightful information about electron transport properties of CNTs-molecular junctions. Besides this insightful information, one should also consider the effects of interface roughness on the structure and property of the realistic molecular devices.

In this work, we have studied mechanically broken CNTs-molecular junctions and effects of interface roughness on their electron transport properties by a combined theoretical approach that includes molecular dynamics (MD), hybrid density functional theory (DFT), and nonequilibrium Green's function method. Molecular dynamic simulations have been employed to model mechanical stretching processes of the metallic carbon nanotube of different chiralities and to obtain realistic contact geometries for the formation of a broken carbon nanotube−molecule−carbon nanotube junction (CNT−Mol−CNT junction). The statistically and energetically most favorable bonding configuration between the deformed carbon nanotubes and a single cruciform diamine molecule with amide linkers has then been determined by density functional theory calculations. Electron transport in such mechanically broken junctions has been further calculated by means of nonequilibrium Green's function theory. The calculated current−voltage characteristics have been compared with the corresponding experimental results.

II. Molecular Dynamics Simulations

In this study, we have examined three different metallic tubes, namely (9,0), (8,2), and (5,5), using the same methodology described above. To simplify the discussion, we use the (9,0) tube to demonstrate the computational procedures employed and the major conclusions obtained.

We have chosen a 4.26 nm long (9,0) single walled CNT with a single defect (an atomic vacancy site) in the middle along the tube axis to start with. The goal is to stretch it into two parts, and then to reconnect both parts by a single molecule. The whole process is modeled with molecular dynamics simulations, using the multiple time step algorithm.[23] During the simulations, the bonded interatomic interaction is modeled with a many-body Tersoff−Brenner potential,[24] which allows the breaking and reforming of the covalent bonds, while Van

* To whom correspondence should be addressed. E-mail: luo@kth.se.
‡ Hunan University.
† Royal Institute of Technology.
§ University of Science and Technology of China.

10.1021/jp102945v
Published on Web 06/29/2010

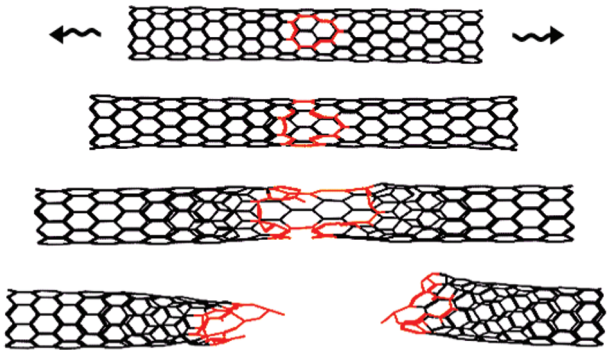

Figure 1. Four snapshots of the mechanical breaking process of a (9,0) tube with a hole defect in the middle of the wall.

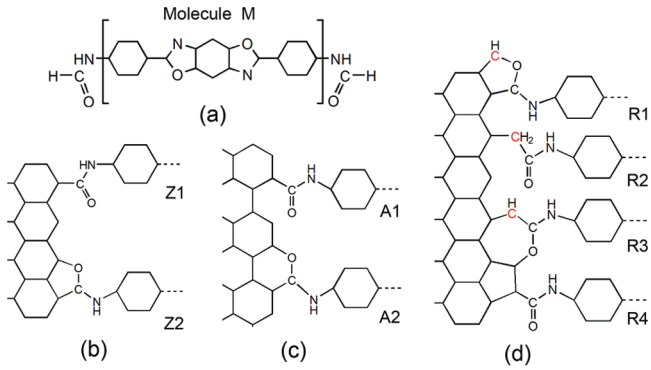

Figure 2. (a) The chemical structure of a single cruciform diamine molecule (M) with two NHOC-H linkers. Schismatical draws of contact geometries between the NHOC-H linker and (b) zigzag or (c) armchair, or (d) irregular edges of BCNTs.

de Waals interaction is described by a Lennard-Jones potential[25] with the cutoff distance of 12 Å. A Nose−Hoover thermostat at room temperature (298 K)[26,27] is considered. The loading of tensile is attained by increasing the tube length step by step. In each loading step, the tube is elongated by 1 Å, and the system is relaxed with fixed ends. After 21 stretching steps, the tube starts to break up near the middle of the tube (right at the position of the single defect) and then the whole stretching process stops when the tube has broken into two parts. Figure 1 shows four snapshots of the stretching processes. From the figure, we can find that the broken areas have pentagon-defects and the broken ends are quite irregular. The edges of the broken ends are mostly of zigzag structure, but the armchair-type and dangling bond of carbon atoms also present randomly. It is noted that the shape of the stretched (9,0) tube obtained from our MD simulations is in good agreement with experimental[17−20] and previous MD simulation[28,29] results.

The irregular ends of broken CNTs (BCNTs) can bring in quite rich connecting structures to form different BCNTs-molecular junctions. To find out the most probable conformation for the system under investigation, we have performed MD simulations again to reconnect the broken CNTs by a single cruciform diamine molecule through its two NHOC-H linkers, see Figure 2a for the chemical structure whose electronic structure can be found in our previous work.[30] During the simulations, the molecule is relaxed in a cubic box with a width of 3.8 nm, which means that the regular part of the BCNTs is fixed and the irregular part is set free in the box. The dehydrogenated linkers NHOC− linkers can be freely attached to the broken edges of BCNTs at any positions. The gap length between two BCNTs is an important factor for the formation of the junction. We have found that when the gap is larger than 2.4 nm, no stable molecular bridge can be found in MD simulations. At the gap length of 2.3 nm, a molecular bridge can form mainly through C−C single bonding contact. When the gap is less than 2.2 nm, polygonal contact geometries can be easily found. At the end, the length of the relaxed molecule M (2.1 nm) is chosen as the gap length, which is also the suggested value in the experiment.[12] We have carried out 100 simulations and in each of them the initial position of the molecule is placed randomly in the box. The statistics of different conformations are given in Table 1. As shown in the table, the BCNTs−molecule provides basically two types of contacts: ideal (regular) and realistic (irregular) contacts. The ideal contact means the ones that can be also found in the ideal CNTs-molecular junctions, as the zigzag (Z1 and Z2) and armchair (A1 and A2) contact geometries shown in Figure 2b and Figure 2c. The realistic contact represents the type of contacts that can only exist in the realistic BCNTs-molecular junctions, which is often introduced by the defects, dangling bond of carbon atoms at the rough edges of broken CNTs. Figure 2d illustrates some of the typical realistic contacts, labeled as R1, R2, R3, and R4, respectively. It should be mentioned that for all these cases, the bridged molecule can be either parallel (P) or titled (T) with respect to the tube axis.

The statistical results have shown that the attached molecule prefers to be titled in the gap though either R1−R3 or R2−R2 local contacts and to form R(9,0)−R1R3/T or R(9,0)−R2R2/T junctions. It is worthy of note that the structure of rough ends, in particular the apex at the end of the BCNTs, plays an important role in the formation of these contacts. For example, a dangling bond of a carbon atom together with a pentagon-defect presented at the apex of the tube at the right (shown in Figure 2d) can favor the formation of the contacts R3 or R2, meanwhile only R1 and R2 are allowed to form on the left BCNTs through a dangling bond of the carbon atom at the apex, but not R3 as the statistics given in Table 1 show.

III. Quantum Chemical Calculations

After the most favorable conformations are obtained, geometry optimization for the entire R(9,0)−R1R3/T junction (total of 437 atoms) and R(9,0)−R2R2/T junction (total of 439 atoms) has been performed, using hybrid density functional B3LYP with 6-31G basis set as implemented in the Gaussian 03 package.[31] Hydrogen atoms have been used to saturate the dangling bonds. Calculations have shown that the binding energy between BCNTs and the molecule for different contacts is of the following order: R1 > R3 > R2 ≫ R4. Therefore, the junctions with R1−R3 contacts are statistically and energetically favorable, whose fully optimized geometry is illustrated in Figure 3a. The molecule is linked to dangling carbon atoms to form a 5-member ring at the left and to form a 7-member ring at the right. Moreover, ideal junctions of I(9,0)−Z1Z1/P, I(9,0)−Z2Z2/P, and I(9,0)−Z2Z2/T have also been optimized at the same level for comparison.

IV. Nonequilibrium Green's Function Calculations

We can now construct the device by connecting the entire BCNTs-molecular junction to two semi-infinity Al leads, as shown in Figure 3. Electron transport properties of constructed devices are simulated with use of the ATK[32,33] package. A supercell is used that contains two layers of a 5 × 5 (100) Al slab with 25 atoms per unit cell in each side, and the entire BCNTs-molecular junction. The use of such a big supercell allows us to uniformly describe the coupling between the molecule and BCNTs, the coupling between BCNTs and Al

TABLE 1: Statistics of Possible Contact Geometries between the Molecule and the Broken (9,0) Tube[a]

	Z1		Z2		A1		A2		R1		R2		R3		R4		sum	
contact	P	T	P	T	P	T	P	T	P	T	P	T	P	T	P	T	P	T
Z1	0	0	0	0	0	0	0	0	0	0	1	2	2	3	0	1	3	6
Z2	1	2	1	1	0	1	0	0	1	2	0	0	1	1	1	2	5	9
A1	0	0	0	0	1	0	0	1	0	0	0	2	0	1	0	0	1	4
A2	0	1	0	0	0	0	0	0	0	2	0	0	0	0	1	1	1	4
R1	1	2	0	3	0	0	1	1	0	1	1	3	6	16	1	2	10	28
R2	0	1	0	1	0	0	0	0	0	0	5	10	1	4	0	0	6	16
R3	0	0	0	0	0	0	0	0	0	0	0	0	0	0	0	0	0	0
R4	0	1	0	0	0	0	0	0	0	1	0	1	1	2	0	1	1	6
sum	2	7	1	5	1	1	1	2	1	6	7	18	11	27	3	7	27	73

[a] Both sides of the junction can be a combination of ideal contacts with zigzag (Z1 and Z2) and armchair (A1 and A2) edges, or realistic (irregular) contacts (R1, R2, R3, and R4). Parallel (P) or tilted (T) conformations of the molecular bridges can both be involved.

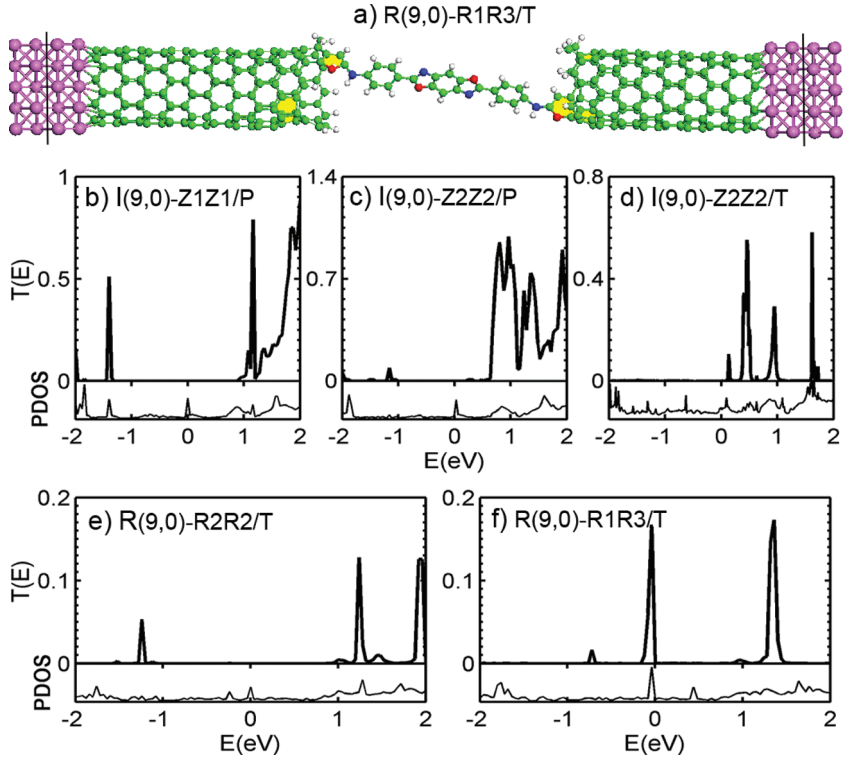

Figure 3. (a) Optimized structure of the junction R(9,0)−R1R3/T. The transmission spectra $T(E, V_b)$ and the partial density of states (PDOS) at the zero bias ($V_b = 0$) for ideal junctions (b) I(9,0)−Z1Z1/P, (c) I(9,0)−Z2Z2/P, and (d) I(9,0)−Z2Z2/T, as well as for realistic junctions (e) R(9,0)−R2R2/T and (f) R(9,0)−R1R3/T, respectively.

leads, and the electronic structure of the entire scattering center. It is noted that it is straightforward to use infinite CNTs as electrodes. The use of Al electrodes allows us to study the performance of real devices at nanoscale. And in order to focus on the realistic contacts between BCNTs and the molecule, we chose a perfect contact between Al lead surface and BCNTs sidewall, and the distance is set to be 0.18 nm.[5−7]

The transmission spectra $T(E, V_b)$ and the partial density of states (PDOS) at the zero bias ($V_b = 0$) for ideal junctions I(9,0)−Z1Z1/P, I(9,0)−Z2Z2/P, and I(9,0)−Z2Z2/T, as well as for realistic junctions R(9,0)−R2R2/T and R(9,0)−R1R3/T, are displayed in Figure 3, panels b, c, d, e, and f, respectively. It can be seen that for ideal molecular junctions, transmission peaks shift with respect to the change of the conformations. It is interesting to note that a strong PDOS peak appears right at the Fermi level of the I(9,0)−Z1Z1/P junction, but without contributing to the transmission spectrum. Such a state is apparently a localized nonconductive state. Our calculations confirm previous observations that the low-energy conduction property of the junction could be dramatically modified by changing the topology of the contacts from a single C−C bond (Z1) to a five-member ring (Z2).[15] In this case, the first transmission and PDOS peak of the I(9,0)−Z2Z2/P junction moves toward the Fermi level. The titled conformation of the molecule can have even stronger effects on the conductance of the junction,[35] as clearly demonstrated by the results shown in Figure 3d for the I(9,0)−Z2Z2/T junction. Our early study showed that in the titled conformation the C−N−O contacting angle is often smaller than that in the parallel conformation, which can lead to stronger hybridization at the contact point that helps the delocalization of molecular orbitals, hence improves the conductivity of the entire system.[30]

For realistic molecular junctions, two favorable conformations R(9,0)−R2R2/T and R(9,0)−R1R3/T have been considered in this study. From Figure 3e, one can find that R(9,0)−R2R2/T is a typical semiconductor and its transmission peak has very low intensity. This behavior can be well understood by looking at its connecting details in Figure 2d. The contact at each side of the R(9,0)−R2R2/T junction is a saturated group $-CH_2-$. It breaks the π conjugation between BCNTs electrodes and the

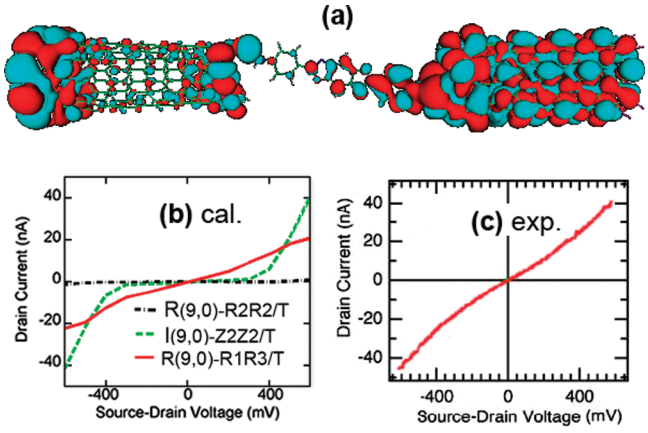

Figure 4. (a) The molecular projected self-consistent Hamiltonian (MPSH) of the highest occupied molecular orbitals (HOMO) of R(9,0)−R1R3/T junction. (b) The calculated current−voltage curves ($I-V$) of I(9,0)−Z2Z2/T, R(9,0)−R2R2/T, and R(9,0)−R1R3/T junctions. (c) The experimental current−voltage curve of a realistic BCNTs-molecular junction.[12]

molecule, resulting in very weak conductance. While in the case of R(9,0)−R1R3/T, which is the one with the most favorable conformation, the situation is different. A transmission peak protrudes to the right at the Fermi level as shown in Figure 3f, suggesting a metallic behavior. By comparing realistic junctions with ideal junctions, one can find that the intensity of T(E) in realistic junctions is much lower than that of ideal junctions. It shows that the deformations and defects on the wall and the rough ends of BCNTs are disadvantageous to the electronic transport. However, the deformations and defects, especial the irregular edge, also bring in rich contacts to the system and renormalize the original electronic structure of the molecule.[34] For instance, it can bring a conducting molecular state closer to the Fermi level of the R(9,0)−R1R3/T junction, resulting in metallic characteristics.

Current−Voltage Characteristics. The molecular projected self-consistent Hamiltonian (MPSH) of the highest occupied molecular orbital (HOMO) of the R(9,0)−R1R3/T junction at zero bias is plotted in Figure 4a. It can be seen that the HOMO covers the entire system and shows highly delocalized characteristics. The conducting HOMO is located about 0.036 eV below the Fermi level and also corresponds to the transmission peak appearing at the Fermi level as shown in Figure 3f. The presence of such a strong conducting orbital is responsible for the metallic behavior of the junction. The current−voltage ($I-V$) characteristics for junctions I(9,0)−Z2Z2/T, R(9,0)−R2R2/T, and R(9,0)−R1R3/T are plotted in Figure 4b, while the experimentally measured $I-V$ curve for a realistic BCNTs-molecular junction[12] is given in Figure 4c for comparison. It is found that the current of ideal junction I(9,0)−Z2Z2/T is close to zero at low bias and starts to change at $V_b = \pm 0.38$ V, showing typical semiconductor characteristics. In the realistic junction R(9,0)−R2R2/T, the contact R2 ($-CH_2-$) totally breaks down the π conjugation of the system, so no current flows in the bias region we have considered, while for the R(9,0)−R1R3/T junction with the most favorable conformation, the current almost linearly increases with the increase of the external bias and the slop is quite large. This confirms that such a junction has strong metallic characteristics. It also should be noted that due to the asymmetric structure, the $I-V$ curve shows slight asymmetric behavior. The predicted asymmetric feature and metallic characteristics of the realistic junction R(9,0)−R1R3/T fit well with $I-V$ characteristics which are measured in the experiments. However, in a general way, the absolute current calculated within the NEGF+DFT framework cannot be directly used to compare with the experimental measured current.

V. Dependence on Chirality

One important parameter that can be used to distinguish different metallic CNTs is the chirality of the tube. Since a (9,0) tube, (n,0) in general, has the minimal chiral angle of value zero, we have chosen a (8,2) tube with a chiral angle of 10.89° and a (5,5) tube with a maximal chiral angle of 30° to examine whether the conformation and the electronic transport properties of junctions depend on the chirality. We have respectively calculated the structure and conductivity of (8,2) and (5, 5) based BCNTs-molecular junctions using the same computational procedures as adopted for the (9,0) tube. MD simulations have again been employed to model the stretching processes of defected (5,5) and (8,2) CNTs. It is found that they are basically broken up along the chiral angle of the tube, see Figure 5, panels a and e. This rule certainly applies to the (9,0) tube with a chiral angle of zero. Such a finding is quite remarkable since it can help experimentalists to determine actual structures of the broken CNTs under mechanical stretching.

MD simulations have also shown that the edge of the broken tube becomes more regular with the increase of the chiral angle. However, even for a (5,5) tube, the broken ends are still largely irregular with mostly zigzag edges, the armchair-type still appears at some points within zigzag arrangements. In any case, the contact topology between the molecule and electrodes becomes relatively simpler. It has been found that the molecule prefers to reconnect both broken (8,2) and (5,5) tubes through Z2−A2 contact geometries with tilted conformation. The optimized structures are given in Figure 5, panels a and e, respectively. Recently, Bruque et al.[22] have studied a (7,7)-molecular junction, for which a (7,7) tube was cut along its chirality angle artificially, but retained two armchair edges at the apex of each broken end. The contact they used has a form of A1-A1, which is one of ideal contacts listed in Table 1. For our realistic (5,5)-molecular junction, the most favorable contact obtained from MD simulations has a form of Z2−A2, which is very different from the ideal A1−A1 contact.

We have calculated transmission spectra for ideal junctions I(8,2)−Z2Z2/T and I(5,5)−A2A2/T, and realistic junctions R(8,2)−Z1Z1/T, R(8,2)−Z2A2/T, R(5,5)−Z1Z1/T, and R(5,5)−Z2A2/T. The results are shown in Figure 5. The (5,5) and (8,2) tubes are not largely deformed during the stretching, the transmission intensities of conducting orbitals in realistic junctions are very close to the ideal junctions. Most importantly, one can see that both realistic junctions R(8,2)−Z2A2/T and R(5,5)−Z2A2/T have a transmission peak right at the Fermi level, showing possible metallic characteristics, while for ideal junctions I(8,2)−Z2Z2/T and I(5,5)−A2A2/T the former shows a possible semiconducting feature and the latter shows possible metallic behavior.

Current−voltage ($I-V$) characteristics of these junctions are calculated and the results are given in Figure 6. Indeed, the $I-V$ curves of junctions R(8,2)−Z2A2/T and R(5,5)−Z2A2/T show obvious metallic behavior, just like the realistic junction R(9,0)−R1R3/T. It is important to mention that we have calculated three realistic CNTs-molecular junctions with most favorable conformation, and all show obvious metallic behavior independent of the chirality of the metallic tubes, while for ideal CNTs-molecular junctions, only I(5,5)−A2A2/T is metallic, but two others are semiconductors. In other words, the conducting behavior of the junction evidently depends on the chirallity of

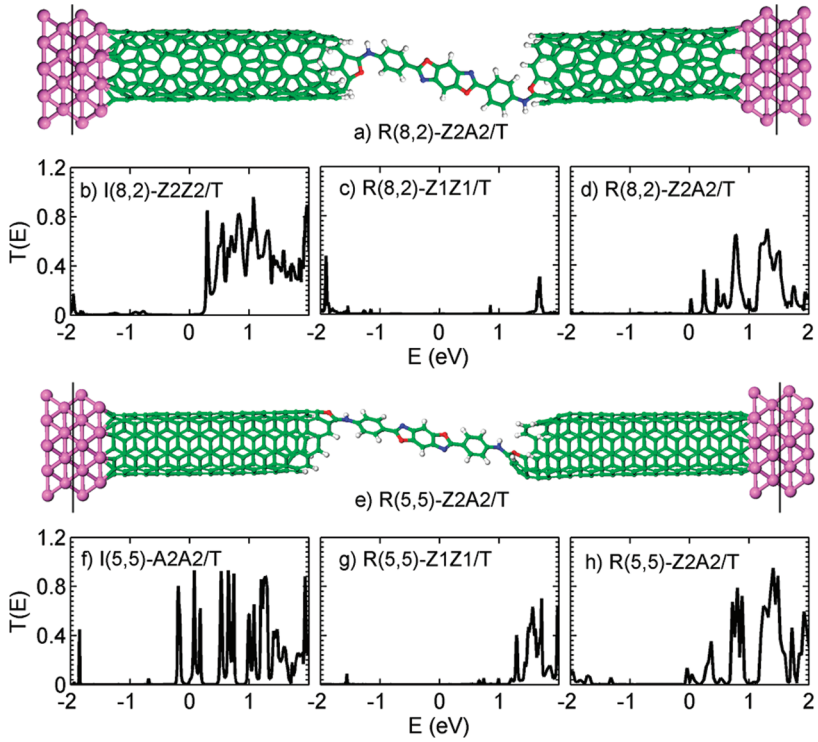

Figure 5. (a) Optimized structure of junction R(8,2)−Z2A2/T. (b, c, d) Transmission spectra $T(E)$ of the junctions I(8,2)−Z2Z2/T, R(8,2)−Z1Z1/T, and R(8,2)−Z2A2/T at zero bias, respectively. (e) Optimized structure of junction R(5,5)−Z2A2/T. (f, g, h) Transmission spectra $T(E)$ of the junctions I(5,5)−A2A2/T, R(5,5)−Z1Z1/T, and R(5,5)−Z2A2/T at zero bias, respectively.

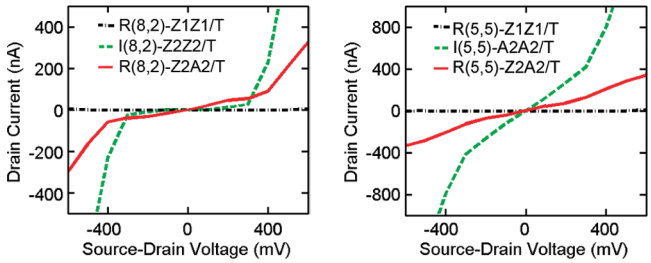

Figure 6. Current−voltage curves for (left) I(8,2)-Z2Z2/T, R(8,2)-Z1Z1/T, and R(8,2)-Z2A2/T junctions and (right) I(5,5)-A2A2/T, R(5,5)-Z1Z1/T, and R(5,5)-Z2A2/T junctions.

CNTs electrodes. It is noted that previous experimental study[12] has shown that a CNTs-molecular junction could recover the original metallic or semiconducting behavior of CNTs with much reduced values of current, which is exactly what we have observed for realistic junctions. This is mainly due to the fact that with the realistic contact geometry the stress in the junction is largely released and the molecule can be naturally bonded to the tubes. In other words, the molecule can act as an extension of the carbon nanotubes through the C−C bonds, recovering the original electrical behavior of CNTs. The combined computational approaches employed in this study can indeed provide good descriptions for the contact structures of the junctions as well as their electron transport properties. The calculated $I-V$ curves for realistic CNTs-molecular junctions have shown that the conductance follows the order R(9,0)−R1R3/T < R(8,2)−Z2A2/T < R(5,5)−Z2A2/T, indicating that the use of armchair tube C(n,n) as electrodes can obtain better conductance.

VI. Conclusions

We have investigated the electronic transport properties of molecular junctions constructed by a single cruciform diamine molecule bridging between two broken metallic SWCNTs. Molecular dynamic simulations have been employed to model the mechanical stretching process of a CNT and the reconnecting process of the broken tubes by a single cruciform diamine molecule. Calculations have shown that the defected CNT breaks along its chiral angle under the mechanical stretching. The broken ends are largely irregular with a mixture of zigzag structure, armchair structure, and dangling bonds of carbon atoms. It is found that the geometry of the rough edge, especially the apex at the ends, plays an important role in the formation of the junction. First-principles calculations have been carried out for statistically and energetically favorable junctions and the calculated results indicate that a CNTs-molecular junction always shows metallic behavior when a metallic CNT is used as the electrode. It is also found that an armchair CNT could be a better choice of electrode for CNTs−molecular junction. These new findings could be useful for the understanding and the design of CNT-based molecular junction or tips of atomic force microscopy.

Acknowledgment. We acknowledge support from the Swedish Research Council (VR), the Swedish National Infrastructure for Computing (SNIC), the National Natural Science Foundation of China (Nos. 10674044, 60871065, 20925311), and the Major State Basic Research Development Programs of China (2010CB-923300), as well as the China Scholarship Council (CSC).

References and Notes

(1) Tour, J. M.; Reinerth, W. A.; Jones, L.; Burgin, T. P.; Zhou, C.-W.; Muller, C. J.; Deshpande, M. R.; Reed, M. A. *Ann. N.Y. Acad. Sci.* **1998**, *852*, 197.

(2) Song, F.; Wells, J. W.; Handrup, K.; Li, Z. S.; Bao, S. N.; Schulte, K.; Ahola-Tuomi, M.; Mayor, L. C.; Swarbrick, J. C.; Perkins, E. W.; Gammelgaard, L.; Hofmann, P. *Nat. Nanotechnol.* **2009**, *4*, 373.

(3) Frank, S.; Poncharal, P.; Wang, Z. L.; de Heer, W. A. *Science* **1998**, *280*, 1744.

(4) Lassagne, B.; Tarakanov, Y.; Kinaret, J.; Garcia-Sanchez, D.; Bachtold, A. *Science* **2009**, *325*, 1107.
(5) Pomorski, P.; Roland, C.; Guo, H. *Phys. Rev. B* **2004**, *70*, 115408.
(6) Xue, Y.; Ratner, M. A. *Phys. Rev. B* **2004**, *70*, 205416.
(7) Li, X.-F.; Chen, K.-Q.; Wang, L.-L.; Long, M.-Q.; Zou, B. S.; Shuai, Z. *J. Appl. Phys.* **2007**, *101*, 064514.
(8) Li, X.-F.; Chen, K.-Q.; Wang, L.; Long, M.-Q.; Zou, B.; Shuai, Z. *Appl. Phys. Lett.* **2007**, *91*, 133511.
(9) Avouris, P.; Chen, Z.; Perebeinos, V. *Nat. Nanotechnol.* **2007**, *2*, 605.
(10) Quinn, B. M.; Lemay, S. G. *Adv. Mater.* **2006**, *18*, 855.
(11) Wilson, N. R.; Macpherson, J. V. *Nat. Nanotechnol.* **2009**, *4*, 483.
(12) Guo, X.; Small, J. P.; Klare, J. E.; Wang, Y.; Purewal, M. S.; Tam, I. W.; Hong, B. H.; Caldwell, R.; Huang, L.; O'Brien, S.; Yan, J.; Breslow, R.; Wind, S. J.; Hone, J.; Kim, P.; Nuckolls, C. *Science* **2006**, *311*, 356.
(13) Guo, X.; Gorodetsky, A. A.; Hone, J.; Barton, J. K.; Nuckolls, C. *Nat. Nanotechnol.* **2008**, *3*, 163.
(14) Ren, W.; Reimers, J. R.; Hush, N. S.; Zhu, Y.; Wang, J.; Guo, H. *J. Phys. Chem. C* **2007**, *111*, 3700.
(15) del Valle, M.; Gutierrez, R.; Tejedor, C.; Cuniberti, G. *Nat. Nanotechnol.* **2007**, *2*, 176.
(16) Ke, S.-H.; Baranger, H. U.; Yang, W. *Phys. Rev. Lett.* **2007**, *99*, 146802.
(17) Huang, J. Y.; Chen, S.; Ren, Z. F.; Wang, Z.; Kempa, K.; Naughton, M. J.; Chen, G.; Dresselhaus, M. S. *Phys. Rev. Lett.* **2007**, *98*, 185501.
(18) Wei, Y.; Jiang, L.; Liu, Z.; Chen; Fan, *Nano Lett.* **2007**, *7*, 3792.
(19) Ziegler, K. J.; Gu, Z.; Shaver, J.; Chen, Z.; Flor, E. L.; Schmidt, D. J.; Chan, C.; Hauge, R. H.; Smalley, R. E. *Nanotechnology* **2005**, *16*, S539.
(20) Gu, Z.; Peng, H.; Hauge, R. H.; Smalley, R. E.; Margrave, J. L. *Nano Lett.* **2002**, 1009.
(21) Bruque, N. A.; Pandey, R. R.; Lake, R. K. *Phys. Rev. B* **2007**, *76*, 205322.
(22) Bruque, N. A.; Ashraf, M. K.; Beran, G. J. O.; Helander, T. R.; Lake, R. K. *Phys. Rev. B* **2009**, *80*, 155455.
(23) Tuckerman, M.; Berne, B. J.; Martyna, G. J. *J. Chem. Phys.* **1992**, *97*, 1990.
(24) Brenner, D. W.; Shenderova, O. A.; Harrison, J. A.; Stuart, S. J.; Ni, B.; Sinnott, S. B. *J. Phys.: Condens. Matter* **2002**, *14*, 783.
(25) Verlet, L. *Phys. Rev.* **1967**, *159*, 98.
(26) Hoover, W. G. *Phys. Rev. A* **1985**, *31*, 1695.
(27) Nose, S. *J. Chem. Phys.* **1984**, *81*, 511.
(28) Li, X.; Yang, W.; Liu, B. *Phys. Rev. Lett.* **2007**, *98*, 205502.
(29) Tang, C.; Guo, W.; Chen, C. *Phys. Rev. Lett.* **2008**, *100*, 175501.
(30) Li, X.-F.; Wang, L.; Chen, K.-Q.; Luo, Y. *Appl. Phys. Lett.* **2009**, *95*, 232118.
(31) Frisch, M. J. *Gaussian 03*, Revision A.1; Gaussian, Inc.: Pittsburgh, PA, 2003.
(32) Taylor, J.; Guo, H.; Wang, J. *Phys. Rev. B* **2001**, *63*, 245407.
(33) Brandbyge, M.; Mozos, J.-L.; Ordejón, P.; Taylor, J.; Stokbro, K. *Phys. Rev. B* **2002**, *65*, 165401.
(34) Yaliraki, S. N.; Ratner, M. A. *J. Chem. Phys.* **1998**, *109*, 5036.
(35) Quek, S. Y.; Kamenetska, M.; Steigerwald, M. L.; Choi, H. J.; Louie, S. G.; Hybertsen, M. S.; VenkataramanLatha, N. B. *Nat. Nanotechnol.* **2009**, *4*, 230.

JP102945V